The goal of this exercise is to consolidate the knowledge you learned in Chapter 5 and to explore in details a central pump-probe experiment [1, 2] in ultrafast spectroscopy and attosecond science.

1 Mathematical description of ultrashort laser pulses

An ultrashort laser pulse can usually be written as a product of a time varying envelope $A(t)$ and a periodic function with angular frequency ω_0:

$$E(t) = A(t)\cos(\omega_0 t + \varphi_{\mathrm{CE}}), \tag{1}$$

where φ_{CE} denotes the phase offset between the carrier wave and the envelope function $A(t)$. In many textbooks, people usually use an *analytical* electric field $\tilde{E}(t) = A(t)e^{i(\omega_0 t+\varphi_{\mathrm{CE}})}$ with the real, physical electric field $E(t) = \frac{1}{2}(\tilde{E}(t) + \tilde{E}^*(t))$ which is very convenient for complex analysis. We would use the second definition later in this exercise.
The spectral amplitude of the pulse is obtained by Fourier transforming the electric field,

$$E(\omega) = \mathfrak{F}[E(t)] = \int_{-\infty}^{\infty} E(t)e^{-i\omega t}\mathrm{d}t, \tag{2}$$

and vice versa, the inverse transform is

$$E(t) = \mathfrak{F}^{-1}[E(\omega)] = \frac{1}{2\pi}\int_{-\infty}^{\infty} E(\omega)e^{i\omega t}\mathrm{d}\omega. \tag{3}$$

Pulses with $|E(\omega)| = E(\omega)$ are called *chirp-free* or *Fourier-limited* pulses.

In addition, it is convenient to approximate the envelope function by a Gaussian:

$$A(t) = A_0 e^{-4\ln 2\left(\frac{t}{T_{\mathrm{FWHM}}}\right)^2}, \tag{4}$$

with A_0, T_{FWHM} being the maximum amplitude and the full width at half maximum of the electric field envelope. The maximum peak intensity is $I = \epsilon_0 cnA_0^2$ and the cycle averaged intensity is $I_{\mathrm{averaged}} = \frac{1}{2}\epsilon_0 cnA_0^2$, with ϵ_0, c, n being the vacuum permittivity, velocity of light, and refractive index of the medium.

1.1 Show that for a Gaussian pulse as above, there exists a relation (time-bandwidth product): $\Delta t\Delta\omega = 4\ln 2$ with $\Delta t = T_{\mathrm{FWHM}}/\sqrt{2}$ being the duration of the intensity envelope $A(t)^2$ and $\Delta\omega$ being the full width at half maximum of the spectral intensity $S(\omega) = |E(\omega)|^2$ of the pulse.

Now we consider a linear property of an ultrashort laser pulse: the propagation through transparent media in the weak field regime. After passing through a medium with refractive index $n(\omega)$ and length L, a laser pulse will accumulate a spectral phase

$$\varphi_m(\omega) = k(\omega)L = \frac{\omega}{c}n(\omega)L. \tag{5}$$

If we do a Taylor expansion of this phase around ω_0

$$\varphi_m(\omega) = \varphi(\omega_0) + \varphi'(\omega_0)(\omega-\omega_0) + \frac{1}{2}\varphi''(\omega_0)(\omega-\omega_0)^2 + \frac{1}{6}\varphi'''(\omega_0)(\omega-\omega_0)^3 + etc., \tag{6}$$

and correspondingly $\varphi'(\omega_0), \varphi''(\omega_0), \varphi'''(\omega_0)$ are called *group delay, group delay dispersion, third order dispersion* and so on.

1.2 Prove that if we apply the *group delay, group delay dispersion* to a *chirp-free*, Gaussian laser pulse, the first term corresponds to a shift in time, the second term corresponds to a broadening of the pulse in time. Often in the laboratories, we encounter cases where the laser pulses are not chirp-free and we want to compress them (i.e. making them shorter, closer to the Fourier-limited duration) by utilizing dispersion.
More details on ultrashort laser pulses in particular and ultrafast optics in general can be found in [3, 4, 5, 6].

2 Generation of ultrashort laser pulses

From the relation derived in 1.1, it is clear that a shorter pulse would generally require a broader bandwidth. In this regard, the titanium-sapphire (Ti:Sa) laser plays a very important role since it could provide high damage threshold and ultrabroad emission bandwidth that can be pumped by powerful green lasers. The first Ti:Sa laser was realized by P.F. Moulton [7] in 1986, the first Kerr-lens mode-locked Ti:Sa laser was realized by Spence et al. in 1991 [8].

2.1 The cavity mode spacing $\Delta\nu$ for a cavity length L is defined as: $\Delta\nu = \frac{c}{2L}$. Now consider two different laser media:

a) A helium-neon gas mixture with $\Delta\nu = 1.5\,\text{GHz}$ gain bandwidth centered around 632.8 nm.

b) A titanium-sapphire crystal with a $\Delta\lambda = 340\,\text{nm}$ wide gain profile centered at 800 nm.

How many longitudinal cavity modes will be amplified within the FWHM of an assumed Gaussian gain profile? Sketch the output spectrum for both lasers schematically.

2.2 Let's switch to the time domain now:
What does the laser intensity look like for an arbitrary phase relation between the different modes? If all modes are oscillating in phase, what does it look like?
Sketch the laser intensity in the time domain for both lasers schematically. Determine the shortest (mostly Fourier limited) pulse duration and the repetition rate for both laser designs.

2.3 Consider a Ti:Sa laser with 75 MHz repetition rate and 6 fs pulse duration. The average output power is 500 mW.
Calculate the energy per pulse. Determine the ratio (peak power)/(average power) and compare the result to the number of modes calculated in 1.2. and derive the relation.

3 Pump-probe experiments and attosecond pulses

3.1 Sketch a typical beam path for a pump-probe experiment and label the optical elements and the important dimensions (for example, optical path length, temporal resolution).

3.2 You would like to probe dynamics with 10 as resolution. Calculate the necessary path length change per delay step of the pump-probe setup.

3.3 What are the limiting experimental factors defining the time resolution in pump-probe experiments?

3.4 One would like to generate optical pulses, which are shorter than 1 fs. Explain how this might be achieved with the carrier wave in the visible part of the electromagnetic spectrum (*Hint:* you might have to abandon the Gaussian approximation of the electric field, see more details in [9]). How would this requirement be relaxed if the carrier wave is in the XUV domain ($\lambda < 100$ nm)?

4 Reconstruction of attosecond beating by interference of two-photon transitions (RABITT)

In the group of Prof. Hans Jakob Wörner we have a setup to perform RABITT experiments. We will show you the laser system and the experimental setup and give a short overview about the research topics in this lab. For preparation please read the following publication:
K.Varjú et al. "'Experimental studies of attosecond pulse trains"', LASER PHYSICS, volume 15 (2005) issue 6, page 888-898 (2005).

While reading make notes to the following questions.

4.1 Describe in your own words how an attosecond pulse train is generated (three-step model).

4.2 List the main components needed for the production of intense few-cycle near-infrared pulses.

4.3 How is the XUV-pulse train separated from the fundamental IR-field?

4.4 Describe why oscillating sidebands occur in a RABITT measurement.

4.5 Think about applications for the RABITT technique considering the experimentally accessible parameters shown in the paper.

References

[1] P. M. Paul, "Observation of a Train of Attosecond Pulses from High Harmonic Generation", *Science*, Vol. 292, pp. 1689–1692 (2001).

[2] H. G, Muller, "Reconstruction of attosecond harmonic beating by interference of two-photon transitions", *Applied Physics B*, Vol. 74, pp. s17-s21 (2002).

[3] A. Weiner, "Ultrafast optics", *John Wiley & Sons, Inc.* (2009).

[4] F. Träger, "Springer Handbook of Lasers and Optics", *Springer Verlag* (2012).

[5] J-C. Diels and W. Rudolph, "Ultrashort laser pulse phenomena", *Elsevier* (2006).

[6] C. Rulliere, "Femtosecond laser pulses", *Springer Verlag* (2005).

[7] P. F. Moulton, "Spectroscopic and laser characteristics of Ti:Al_2O_3", *JOSA B*, Vol. 3, Issue 1, pp. 125-133 (1986).

[8] D. E. Spence, P. N. Kean, and W. Sibbett, "60-fsec pulse generation from a self-mode-locked Ti:sapphire laser", *Optics Letters*, Vol. 16, Issue 1, pp. 42-44 (1991).

[9] M. Th. Hassan, T. T. Luu, A. Moulet, O. Raskazovskaya, P. Zhokhov, M. Garg, N. Karpowicz, A. M. Zheltikov, V. Pervak, F. Krausz and E. Goulielmakis, "Optical attosecond pulses and tracking the nonlinear response of bound electrons", *Nature*, Vol. 530, pp. 66-70 (2016).

Laser Physics, Vol. 15, No. 6, 2005, pp. 888–898.

Experimental Studies of Attosecond Pulse Trains

K. Varjú[1], P. Johnsson[1], R. López-Martens[1], T. Remetter[1], E. Gustafsson[1], J. Mauritsson[2], M. B. Gaarde[2], K. J. Schafer[2], Ch. Erny[3], I. Sola[4], A. Zaïr[4], E. Constant[4], E. Cormier[4], E. Mével[4], and A. L'Huillier[1, *]

[1] *Department of Physics, Lund Institute of Technology, P.O. Box 118, SE-22100 Lund, Sweden*
[2] *Department of Physics and Astronomy, Louisiana State University, Baton Rouge, Louisiana 70803-4001, USA*
[3] *Physics Department, Swiss Federal Institute of Technology (ETH Zürich), CH-8093 Zurich, Switzerland*
[4] *CELIA, Université Bordeaux 1, 351 Cours de la Libération, 33405 Talence, France*
*e-mail: anne.lhuillier@fysik.lth.se
Received February 4, 2005

Abstract—We present experimental measurements of attosecond pulse trains. The characterization of the pulses uses a spectral interferometry technique that is implemented with a Mach–Zehnder interferometer. This allows us to manipulate independently the pump and probe pulses for a wide range of applications. By letting the attosecond pulses pass through metallic films, we can in particular compensate for the intrinsic chirp of the attosecond pulses corresponding to the plateau spectral region, thus getting pulses as short as 170 attoseconds—only 1.2 optical cycles at the central frequency. The measurement technique is also applicable for determination of the group delay of thin XUV-transparent films and relative delay in the photoionization process. Our experimental method is applied to attosecond pulse trains created by 35- and 9-fs laser pulses, and the shortest train observed consists of three or four pulses.

1. INTRODUCTION

The production of short light pulses requires a large spectral bandwidth where all the spectral components of the radiation add constructively during a very short instant of time. More than ten years ago, the process of high-order-harmonic generation in intense laser fields [1], which provides a large spectral bandwidth in the extreme ultraviolet (XUV) range, was proposed as a possible candidate for the production of attosecond pulse trains (APT) [2, 3]. Only recently have techniques been developed to measure the duration of subfemtosecond XUV pulses. The most direct method is a nonlinear autocorrelation technique exploiting two-XUV-photon ionization in the time domain. It requires, however, a high XUV intensity, which has been achieved so far only for low process orders. By spectrally filtering the 7th to the 15th harmonics generated in xenon, the production of trains of 780-as pulses has been demonstrated using this technique [4]. Cross-correlation techniques where the XUV pulse is probed by the infrared laser field scale linearly with the XUV intensity and can therefore be used over a broader spectral range. The attosecond streak camera method exploits the dependence of the kinetic energy of the XUV-pulse-generated photoelectron on the phase of the laser field at the instant of photoionization. This method has been used to demonstrate the production of single attosecond pulses with durations down to 250 as [5, 6, 7]. These pulses are obtained by making a rather abrupt spectral selection of harmonics in the cutoff region and by using phase-stabilized few-cycle driving lasers [8]. Another cross-correlation method, namely, resolution of attosecond beating by interference of two-photon transitions (RABITT) is based on mixed-color ionization involving one XUV photon and one driver laser photon [9–11]. It is a simple and versatile spectrally based method that is useful for the characterization of trains of attosecond pulses.

The production of attosecond light pulses using high-order harmonics requires one to limit the spectrum to those harmonics being synchronized and that are comparable in amplitude. A recent systematic RABITT analysis of plateau harmonics generated in argon and neon shows that the frequency components of the XUV radiation are not exactly synchronized and that the XUV pulses consequently exhibit a significant chirp (frequency variation in time) [11, 12]. This intrinsic chirp comes from the fundamental electron dynamics responsible for high-order harmonic generation, as illustrated in Fig. 1. Twice per laser cycle, a wavepacket tunnels through the barrier formed by the atomic potential lowered by the electromagnetic field and is launched into the continuum, where it propagates under the influence of the laser field. Part of the wavepacket is driven back to the core after approximately half a laser cycle and recombines, releasing the excess energy gained in the continuum in the form of a photon. In the time domain, this leads to the emission of short XUV pulses separated by 1.3 fs (half a laser cycle of 800-nm laser radiation), while, in the spectral domain, discrete peaks at odd multiples of the laser frequency appear as a result of the periodicity of the process. The pulses are chirped because different energy components of the wavepacket return to the core at different times. This reduces the optimum bandwidth over which the shortest pulses can be obtained to a few harmonics. In addi-

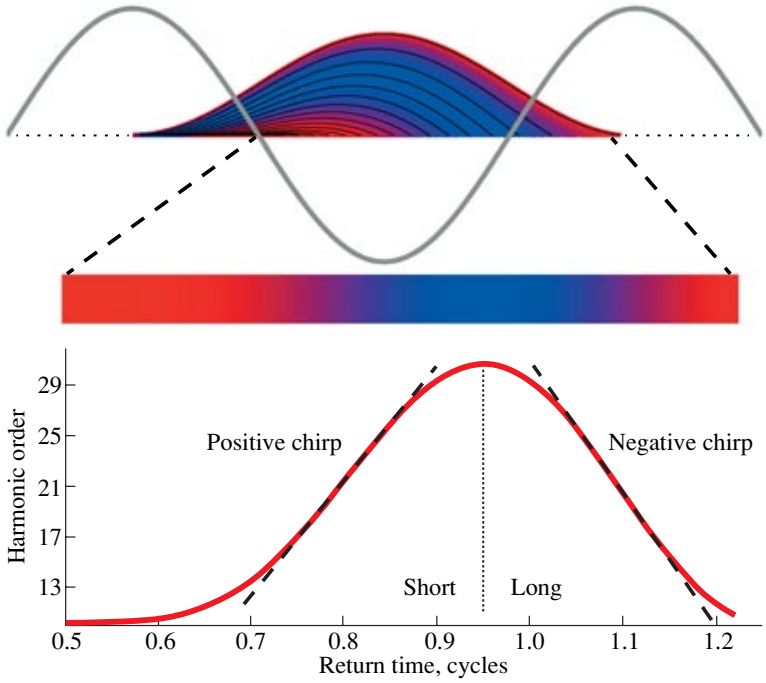

Fig. 1. Illustration of the physics of high-order-harmonic generation. The top figure shows classical electron trajectories for different initial phases relative to the IR laser field (black lines). The electron returns to the atom when it again crosses the horizontal dotted line. The color illustrates the variation of the kinetic energy for the different trajectories (blue means the highest energy). The bottom figure shows the generated harmonic order as a function of the time when the electron returns to the core. This simple calculation shows the existence of a short (left side) and a long (right side) trajectory separated by the cutoff, as well as the frequency variation in time of the attosecond burst.

tion, other parts of the wavepacket, following long quantum paths, return at much later times relative to the instant of ionization and may also lead to emission of XUV radiation, thus further destroying the well-localized attosecond pulse structure. This radiation is more divergent than the former and can be strongly reduced by stopping down the harmonic beam [13, 14]. Obtaining clean attosecond pulses consequently requires spatial filtering as well as accurate amplitude and phase control of the XUV radiation.

In the present paper, we review the recent experimental measurements performed in Lund using the RABITT technique. We have developed a Mach Zehnder type of interferometer that allows us to manipulate independently the pump and probe pulses; this allows us in particular to compensate for the intrinsic chirp of the attosecond pulses corresponding to the plateau spectral region, thus achieving on-target pulses as short as 170 attoseconds. We describe in detail the experimental method and principle of the measurement technique (Section 2). We review some recent results [11], giving additional details on the experiment, and discuss the influence of the phase of the ionization processes on the determination of the pulse duration of attosecond pulses (Section 3). Finally, we present new results recently obtained with ultrashort (sub-10-fs) laser pulses (Section 4).

2. EXPERIMENTAL SETUP AND MEASUREMENT TECHNIQUE

2.1. Laser System

The Lund High-Power Laser Facility of the Lund Laser Center operates a 1-kHz Ti:sapphire laser with the specifications indicated below.

Beam diameter, $1/e^2$	8 mm
Pulse duration	35 fs
Pulse energy	2 mJ @ 1 kHz
Spectral bandwidth	~35 nm

Short pulses are generated using a Kerr-lens mode-locked oscillator, in which the dispersion is controlled by a set of prisms. In order to precisely control the temporal characteristics of the laser pulses and to minimize the gain narrowing, an acoustooptical programmable dispersive light modulator [15], also known as "Dazzler," is used to shape the pulses both spectrally and temporally. Before amplification, the pulses are positively stretched in an Offner triplet stretcher. The first

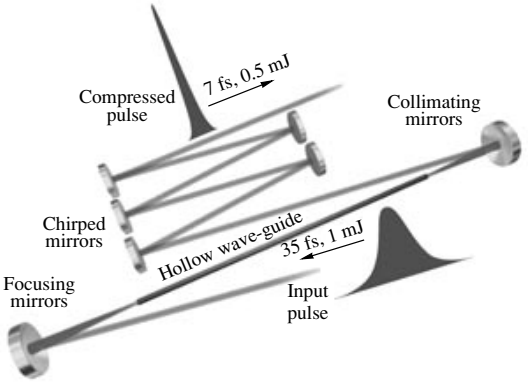

Fig. 2. Schematic illustration of the setup used for laser-pulse postcompression. The capillary is enclosed in a tube with static gas pressure.

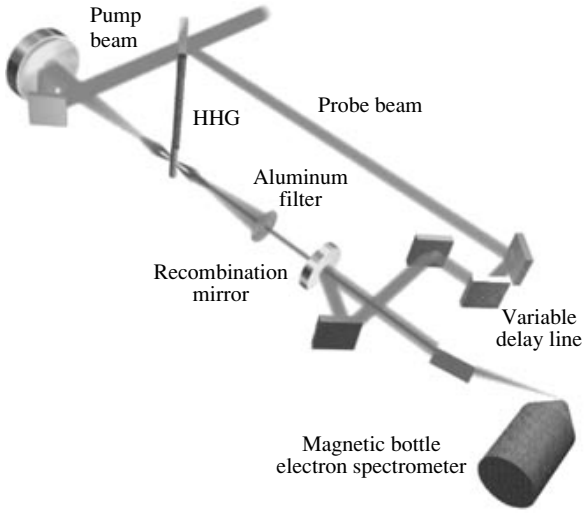

Fig. 3. Experimental setup for the generation, postcompression, and characterization of attosecond pulses (see text for details).

amplification stage is a regenerative amplifier pumped by a Nd:YLF laser, which provides a very high gain and excellent spatial beam quality after amplification. Further amplification is achieved in two double-pass amplifiers. Once the pulses have been amplified, they are compressed in a compressor based on two parallel gratings. By varying the angle of the gratings and the distance between them, the dispersion introduced by the stretcher and by propagation through materials in the amplification process can be compensated for to produce short pulses with significantly higher intensity.

2.2. Postcompression of Laser Pulses

A pulse post-compressor based on a gas-filled hollow waveguide followed by a dispersive line of chirped mirrors [16, 17] has been implemented and used in some applications [18]. This compressor is capable of producing pulses as short as 7 fs with an energy of 0.5 mJ per pulse starting from 1-mJ, 35-fs pulses. However, a smaller amount of energy is often sent to the capillary, which increases the output pulse duration. Very stable 10-fs pulses are routinely produced. The pulse-compression scheme is described in Fig. 2. A 65-cm-long capillary with a 260-μm inner diameter is used to guide the laser pulses. The capillary is usually filled with argon at ~300 mbar. The pulse duration is determined with the help of spectral interferometry for direct electric field reconstruction (SPIDER) measurements [19, 20].

2.3. Harmonic Generation and a Pump–Probe Interferometer

Figure 3 describes how we generate and characterize the attosecond pulses by cross correlation with an infrared pulse. The laser pulse is split in two using a 300-μm thin beam splitter. The (pump) pulse is focused into a 3-mm static argon-gas cell (30 mbar) with a 50-cm spherical mirror. The generated harmonics are spectrally filtered by one (or several) 200-nm-thick aluminum filters. These filters also serve the purpose of eliminating the fundamental IR light. The harmonics are passed from the back through a 1.5-mm hole in the middle of a spherical mirror placed under vacuum and are focused by a platinum-coated toroidal mirror with a 30-cm focal length into the sensitive region of a magnetic bottle electron time-of-flight spectrometer (MBES) or, as in a recent experiment, a velocity-map imaging spectrometer. The probe pulse is sent through a variable delay stage and is recombined with the harmonic pulse after reflection on the holed mirror. The curvature of the spherical mirror is chosen such that the wavefront of the reference beam matches that of the harmonic beam at the focus point inside the spectrometer. This Mach–Zehnder type of interferometer puts a very high demand on the mechanical stability of the system, which we achieve by using vibration damping on all turbomoleculer vacuum pumps and also by isolating all primary pumps. The advantage of this setup over previous arrangements [9, 12], where the pump and probe beams travel collinearly throughout, is the possibility of manipulating both beams independently. This has allowed us, for example, to study the effect of fundamental chirp [18] or varying ellipticity of the fundamental field [21], to change the relative polarization of the cross-correlated beams [22], and to use different durations of the laser and XUV beams [18].

The MBES is filled with a rare gas at a few times 10^{-4} mbar static pressure. Different gases are used in order to cover a large spectral range in the analysis. Kr

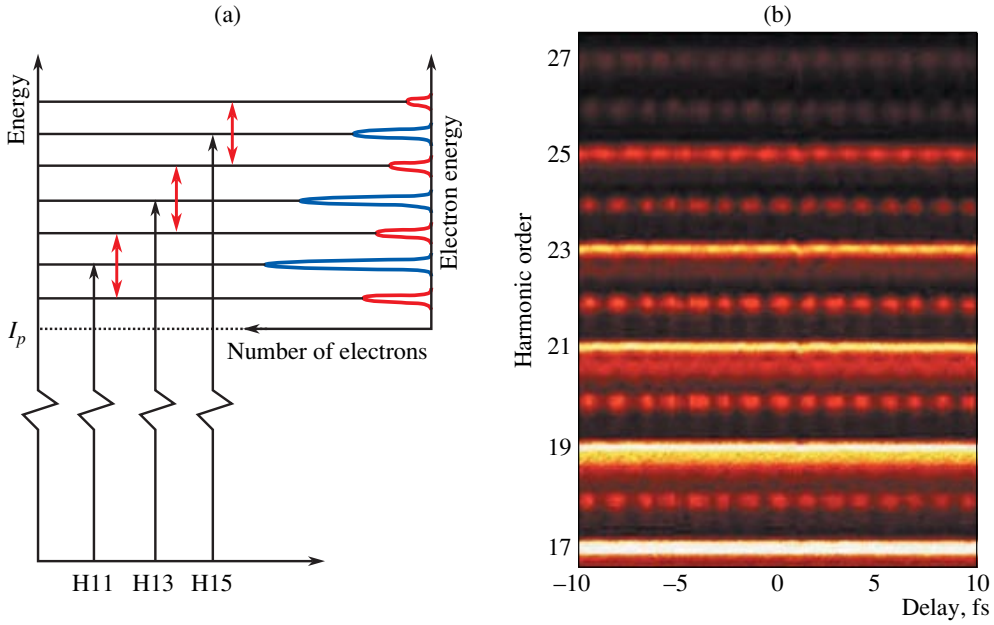

Fig. 4. Principle of the RABITT technique. It consists in measuring a "sideband" signal, which results from the interference between two processes, namely, absorption of a harmonic photon and a probe photon ($q\omega + \omega$) and absorption of a harmonic photon and emission of a probe photon ($(q + 2)\omega - \omega$), as a function of the temporal delay between the pump and probe pulses. On the right we show a RABITT acquisition, i.e., recording of the photoelectron spectra as a function of delay.

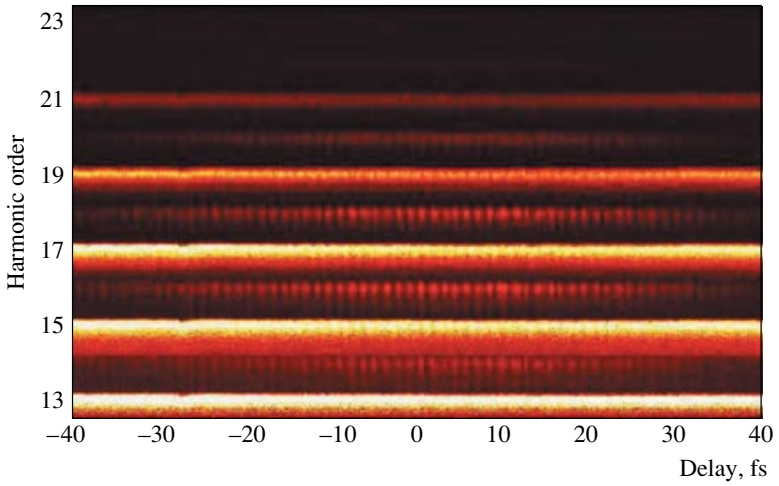

Fig. 5. A typical RABITT acquisition with harmonic and sideband signals (in false colors) is shown as a function of the time delay. We show here the full trace, which enables the complete reconstruction of the APT [34].

and Ar have a relatively low ionization potential and a high cross section for low energies, whereas Ne exhibits a flat but low cross section over a large energy range [23]. When the relatively low-intensity (10^{11} W/cm^2) probe pulse overlaps in time with the harmonic pulses, sidebands appear in the photoelectron spectra, which is due to the absorption of a harmonic and a probe photon as well as to the absorption of the next consecutive harmonic and emission of a probe photon, as illustrated in Fig. 4a. A typical spectrum, plotted as a function of delay, is shown in Fig. 4b. We detect time-of-flight electron signals that are then converted to energy spectra. The energy resolution varies as $E^{-3/2}$, where E is the electron energy. When obtaining this scan, a retarding

potential of 6 V was being applied to the flight tube, which enabled us to resolve a higher energy region. The intensity of the photoelectron signal is represented by colors (from black through red to yellow). The sidebands, which correspond to even harmonic orders, oscillate as a function of delay, exhibiting a high contrast. The harmonic lines do not vary with delay when the harmonic peaks are considerably higher than the sideband peaks in the electron spectrum. On the other hand, towards the cutoff, the XUV intensity is decreasing, and the sideband generation cross section also increases with energy, so the harmonic and sideband peaks become comparable in magnitude. As a result of redistribution between the harmonic and sideband peaks, we observe an oscillation of the harmonics opposite in phase to the sidebands (harmonics 25 and 27 in Fig. 4b). The side structure of intense harmonics (especially 21 of Fig. 4b) is due to saturation of the acquisition system. We also show in Fig. 5 a full trace, which can be used for complete reconstruction of the APT [34].

To understand how these results allow us to determine the duration of attosecond pulses, we now go through the principle of the RABITT technique [24].

2.4. Principle of the RABITT Analysis

Using second-order perturbation theory, the sideband signal is proportional to

$$S(\omega, \tau) \propto \left| \int_{-\infty}^{\infty} [A_{\rm abs} + A_{\rm em}] dt \right|^2, \qquad (1)$$

with

$$\begin{aligned} A_{\rm abs} &= \sum_i \frac{\langle f|er|i\rangle\langle i|er|g\rangle}{\epsilon_i - \epsilon_g - q\omega} E_0(t-\tau) E_q(t) e^{iI_p t}, \\ A_{\rm em} &= \sum_i \frac{\langle f|er|i\rangle\langle i|er|g\rangle}{\epsilon_i - \epsilon_g - (q+2)\omega} E_0^*(t-\tau) E_{q+2}(t) e^{iI_p t}, \end{aligned} \qquad (2)$$

where g, i, and f denote the ground, intermediate, and final states of the two-photon transition, respectively; ϵ_g, ϵ_i, and ϵ_f are the corresponding energies; and E_0 and E_q are the (complex) representations of the probe and harmonic fields, respectively. I_p is the ionization potential, and τ is the delay between the IR and XUV pulses. A summation is performed over the (virtual) intermediate states. For simplicity, we have not written here the expressions for the processes where a probe photon is absorbed or emitted first [9]. We can separate the rapid and slow temporal variations of the light fields as

$$\begin{aligned} E_0(t) &= \tilde{E}_0(t) e^{-i\omega t - i\Phi_0}, \\ E_q(t) &= \tilde{E}_q(t) e^{-iq\omega t - i\Phi_q}. \end{aligned} \qquad (3)$$

Here, Φ_q is the phase of the harmonics at the detection point; therefore, it accounts for the intrinsic phase of the harmonic generation as well as any phase acquired during propagation (including the effect of filters). We introduce the following notations:

$$\begin{aligned} \sum_i \frac{\langle f|er|i\rangle\langle i|er|g\rangle}{\epsilon_i - \epsilon_g - q\omega} &= \tilde{A}_{\rm abs}^q e^{-i\varphi_{\rm abs}^q}, \\ \sum_i \frac{\langle f|er|i\rangle\langle i|er|g\rangle}{\epsilon_i - \epsilon_g - (q+2)\omega} &= \tilde{A}_{\rm em}^{q+2} e^{-i\varphi_{\rm em}^{q+2}}. \end{aligned} \qquad (4)$$

Furthermore, we assume that the probe field is transform-limited, choose the temporal delay so that $\Phi_0 = 0$, and neglect the variation of the harmonic chirp and amplitude between the qth and the $(q+2)$th harmonics [18], so that $\tilde{E}_q(t) \simeq \tilde{E}_{q+2}(t)$. Equation 1 then reduces to

$$S(\omega, \tau) \propto M \left| \int_{-\infty}^{\infty} \tilde{E}_0(t) \tilde{E}_q(t) e^{-i(q+1)\omega t + iI_p t} dt \right|^2, \qquad (5)$$

with

$$M = \left| \tilde{A}_{\rm abs}^q e^{-i\varphi_{\rm abs}^q - i\Phi_q + i\omega\tau} + \tilde{A}_{\rm em}^q e^{-i\varphi_{\rm em}^{q+2} - i\Phi_{q+2} - i\omega\tau} \right|^2. \qquad (6)$$

This term will lead to a modulation of the intensity of the sidebands that is proportional to $\cos(\Delta\varphi_{\rm at}^{q+1} + \Delta\Phi_{q+1} - 2\omega\tau)$, with $\Delta\varphi_{\rm at}^{q+1} = \varphi_{\rm abs}^q - \varphi_{\rm em}^{q+2}$ and $\Delta\Phi_{q+1} = \Phi_q - \Phi_{q+2}$.

Our experiment consists in studying the sideband signal as a function of harmonic order q over a large range of harmonic orders and in recording RABITT traces such as that shown in Figs. 4b and 5. To get the relative phase of the harmonics, the photoelectron signal is integrated over each sideband for every time delay. Using a Fourier-transform method, the absolute phase of the sideband oscillation and, thus, $\Delta\varphi_{\rm at}^{q+1} + \Delta\Phi_{q+1}$, is obtained. Accounting for the atomic phase difference $\Delta\varphi_{\rm at}^{q+1}$, obtained from TDSE calculations [25] and shown in Fig. 6a, the relative phases Φ_q of the harmonics can be obtained by concatenation of the phase differences. We note here that the effect of the atomic phase relative to the delay caused by the harmonic-generation process is rather small. In our case it corrects the attosecond pulse duration by approximately 10 as. Finally, by combining these phase differences with the easily accessible harmonic intensities I_q, which are equal to the ratio of the measured electron peak intensities and the ionization cross section of the

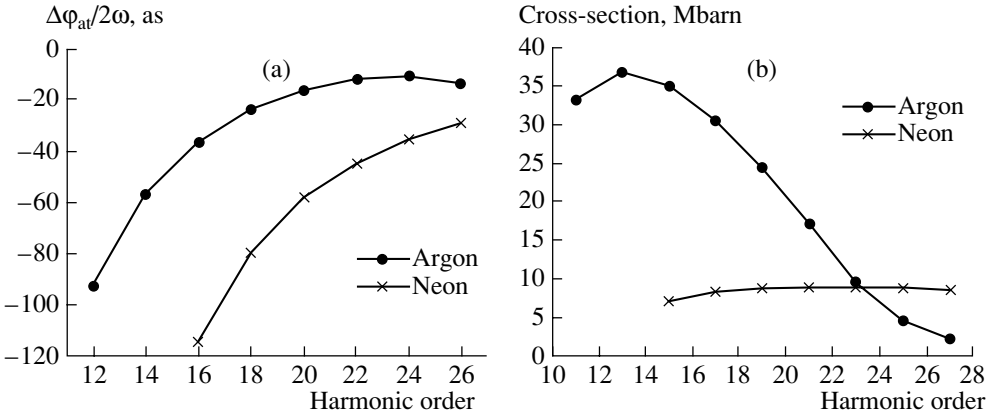

Fig. 6. Calculated $\Delta\varphi_{at}^{q}$ [25] and absorption cross section of argon and neon as a function of q.

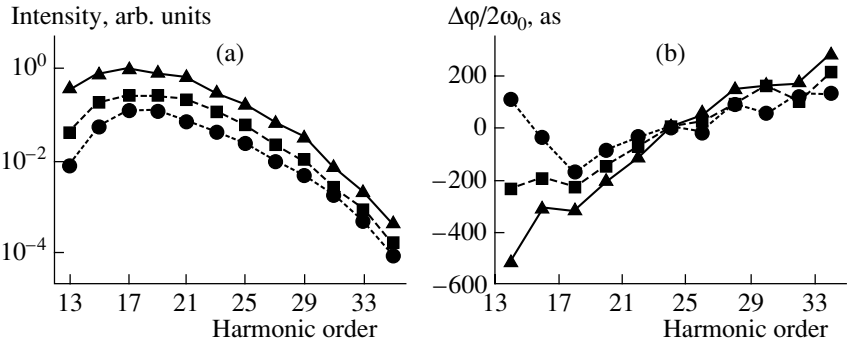

Fig. 7. Harmonic intensities and first-order spectral phase for different numbers of aluminum filters. Solid: one filter, dashed: two filters, dotted: three filters.

detection gas (shown in Fig. 6b), the average pulse in the pulse train can be reconstructed:

$$I(t) = \left| \sum_{q = q_i, q_f} \sqrt{I_q} e^{-iq\omega t - \Phi_q} \right|^2. \quad (7)$$

In this analysis, the harmonics are assumed to be monochromatic, so that the reconstruction does not account for any variations of the pulse characteristics over the pulse train. Mathematically, this follows from neglecting the variation in harmonic chirp and amplitude in the step leading to Eq. (5).

3. ATTOSECOND PULSE TRAINS CREATED BY 35-FEMTOSECOND IR PULSES

3.1. Characterization and Postcompression of Attosecond Pulses

Here, we report on some recent measurements [11] wherein we have not only generated and characterized an attosecond pulse train but also compressed the pulses. Our experimental setup (Fig. 3) includes an aluminum filter that has a triple function: it eliminates the fundamental light generating the harmonics by reflecting it and efficiently cuts the low-order harmonics below the eleventh. Combined with the spectral cutoff in argon at higher frequencies, it then acts as a bandpass filter, which selects a spectrum centered at 30 eV with a total bandwidth of 30 eV. Finally, the transmitted pulses acquire a negative chirp that is opposite in sign to the dispersion of the generation process [11, 12, 26]. Another element in our experimental setup that is important for the generation of trains of short attosecond pulses is the holed recombination mirror, which rids the transmitted harmonic beam of unwanted spectral substructures from longer quantum paths with higher spatial divergence [13, 14].

Three series of measurements have been performed using one, two, or three aluminum filters, each of 200-nm thickness. Figure 7 presents the different results obtained in the three cases for the harmonic intensities (Fig. 7a) and difference of phases (Fig. 7b). Different detection gases, namely, argon and neon, have been here used to cover the full spectral range and to thus characterize the on-target radiation. We correct the

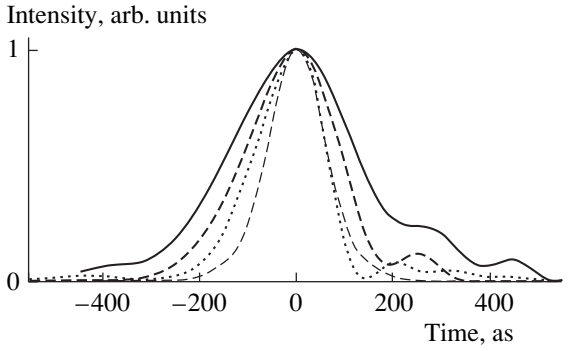

Fig. 8. Average pulses of the train for different numbers of aluminum filters. Thick lines are as in Fig. 7; the thin dashed line is the transform-limited pulse for the given spectrum.

results for the cross section and atomic phase of the gases. The influence of the grazing-incidence toroidal refocusing mirror is found to be negligible. As the number of filters increases, the transmitted spectrum becomes more symmetric (Fig. 7a) and the variation of the delay of the harmonic components, equal to $\Delta\Phi_q/2\omega$ over the investigated bandwidth, decreases (Fig. 7b).

The properties of aluminum, shown in Fig. 9 (dotted line), are interesting for the postcompression of attosecond pulses in the spectral region between the 17th and 27th harmonics, such that the transmission is not too small and the group delay dispersion (double derivative of the spectral phase) is negative and (approximately) constant. Below the 17th harmonic, the Al group delay dispersion (GDD, derivative of the line shown in Fig. 9b) increases rapidly in magnitude, which leads to overcompensation of the chirp in this regime, but the filter transmission (Fig. 9a) is strongly reduced. Above the 27th harmonic, the absolute value of the GDD decreases, and the filter has less of an effect on the temporal properties of the attosecond pulses, which shows up in the experimental results as the invariance of the delay $\Delta\Phi_q/2\omega$ with the number of filters. In our experiments, the peak laser intensity was therefore adjusted to be 1.4×10^{14} W/cm^2 so that this region (above the 27th harmonic) coincides with the spectral cutoff, where, as confirmed by our experimental data, the delay is almost constant [7, 27]. At this generating intensity, the second-order spectral phase $(1/\omega^2\partial^2\Phi/\partial q^2)$ is found to be 2.1×10^{-32} s^2, which is equivalent for our Gaussian pulses to a chirp rate $(1/2\partial^2\Phi/\partial t^2)$ of 3.7×10^{31} s^{-2}. In the harmonic range between the 17th and 27th, we have measured our 200-nm aluminum filters to exhibit an average GDD of -6×10^{-33} s^2. This shows that, in this spectral region, we would need 3.5 filters or, equivalently, a 700-nm filter to completely flatten the delay curve [28]. On the other hand, this would lead to even stronger over-compensation of the low orders. Since our measured pulse duration is rather close to the Fourier transform limit, we consider the compression with three filters to be close to optimum. The appropriate choice for the Al thickness to compensate for the intrinsic chirp in the plateau region and the choice of the laser intensity to tune the cutoff position allow us to flatten the spectral phase of the XUV light over a 30-eV bandwidth, thus enabling the formation of clean and very short (170-as) attosecond pulses.

The reconstructed average attosecond pulses on-target in the different cases (Eq. 7) are shown in Fig. 8. The determined pulse widths are 280 as (1 filter), 220 as (two filters), and 170 as (three filters). The transform-limited pulse width corresponding to the three-filter spectrum is 150 as. Note that 170 as corresponds to only 1.2 cycles of the central frequency (30 eV). By extrapolating to zero filters but still maintaining the same spectral amplitudes as for one filter, we estimate a duration equal to 480 as. Let us also point out that the relatively less-intense high harmonics from the 27th to the 35th are essential to get a short (sub-200 as) duration.

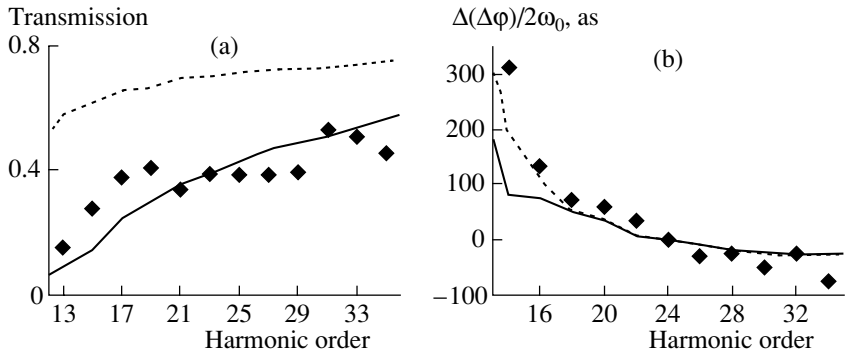

Fig. 9. Transmission and group delay of aluminum films. The symbols are values deduced from measurements; the dotted line is calculated from tabulated values for a film of 200-nm Al. The solid line is the calculation for 185-nm Al with a 15-nm Al_2O_3 layer.

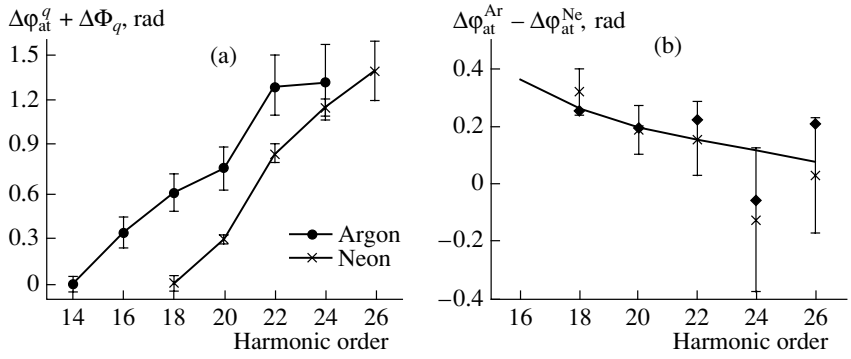

Fig. 10. Phase differences $\Delta\varphi_{at}^{q} + \Delta\Phi_q$ obtained for argon and neon using the same attosecond pulse trains, i.e., for the same $\Delta\Phi_q$ (a). Difference between the measured ($\Delta\varphi_{at}^{q} + \Delta\Phi_q$) values in argon and neon (b). The line represents theoretical results obtained by solving the TDSE. The two symbols represent values obtained from two pairs of scans.

3.2. Application of RABITT Measurements to Determination of Refractive Indices

A comparison between results obtained by using different numbers of similar filters gives information on the spectral response (dispersion and absorption) of aluminum. The homogeneity and thickness of these filters have been carefully verified by scanning electron microscopy. The thickness is measured to be 200 ± 5 nm. Because of the rapid oxidization process, the surface of the filters is unfortunately covered on each side by a thin layer of aluminum oxide. In Fig. 9a, we plot the ratio between experimental harmonic intensities obtained with two and one filters (or, equivalently, three and two filters) and compare it to calculated transmission curves obtained using x-nm Al_2O_3 and $(200 - x)$-nm Al with tabulated values [29, 30]. The best agreement is obtained for 185-nm Al and 15-nm Al_2O_3 (solid line), in agreement with expected oxide thicknesses found in the literature [29]. By comparison, the transmission and group delay through a pure 200-nm Al filter is shown by the dotted line. We show here that the ideal properties of aluminum for the compression of the XUV bursts are considerably reduced by the oxide layer.

Figure 9b shows the difference in spectral phase measurements (i.e., relative group delay) between two and one filters (or, equivalently, three and two filters). Again, the experimental data are compared to calculated group delays for a 200-nm Al filter and for 185-nm Al and 15-nm Al_2O_3 using tabulated data on refractive indices [29, 30]. The fit of the experimental measurements to the relative group delay induced by the aluminum filter (with the oxide layer) is reasonably good, but there is a systematic deviation at low energies. We suspect that this is due to an uncertainty in the refractive indices in this spectral region. Independent measurements of similar Al filters, using an XUV-interferometric method, also indicated a deviation of similar extent from the tabulated refractive-index data [31]. Note that this method can also be used to determine the refractive index of pure aluminum, because the thickness of the oxide layer is independent of the thickness of the filter. Systematic broadband RABITT measurements might be an interesting technique for determining the variation of the refractive indices of metallic filters (close to their absorption edges) in the energy range 10–50 eV, where measurements with other methods are not available [32].

3.3. Influence of Atomic Phases

The electron wavepacket generated via a one-photon ionization process acquires a spectral phase known as the atomic phase [24, 33]. Using the RABITT technique, the phase contributions originating from the APT and the atomic phases are indistinguishable [9]. However, using the same APT but different gases for the RABITT measurements, we can access the variation in the atomic phase between the gases, since the phase of the APT in this case cancels:

$$(\Delta\varphi_{Ar}^{q} + \Delta\Phi_q) - (\Delta\varphi_{Ne}^{q} + \Delta\Phi_q) = \Delta\varphi_{Ar}^{q} - \Delta\varphi_{Ne}^{q}. \quad (8)$$

We have compared RABITT measurements in two gases, namely, Ar and Ne, using very similar experimental conditions and have compared the results with theoretical predictions. The experiments were performed directly after each other in a sequence Ar–Ne–Ar. Very stable argon results confirm that the characteristics of the attosecond pulse train used to ionize the different gases could be considered to be constant. The results are presented in Fig. 10a. The difference of phases, plotted as a function of harmonic order, is proportional to the first-order spectral phase of the (average) attosecond electron wavepacket created by ionization of the detection gas. Only one filter was used, which explains the significant second-order spectral phase. In Fig. 10b, we compare the measured atomic

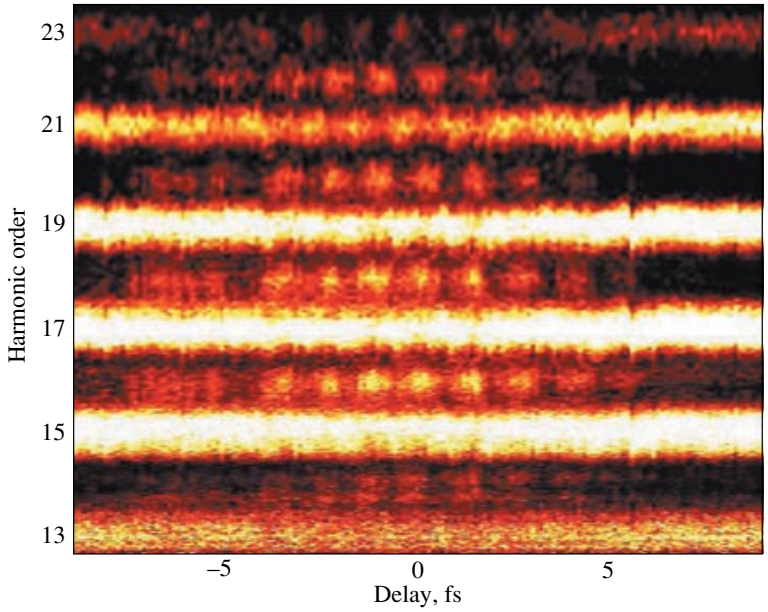

Fig. 11. RABITT scan of the harmonics generated by a 9-fs pulse.

phase variation between Ne and Ar with theoretical data obtained from nonperturbative time-dependent calculations (Fig. 6a). The agreement between the variations of the atomic phase difference with energy to the theoretical curve is reasonably good, considering the rather small extent of the effect. In the present (preliminary) experiment, we did not have the reference to the generating IR pulse [36]; therefore, the phase-difference values are only correct up to a constant vertical shift, and we have arbitrarily set the phase of the lowest sideband to zero. For the same reason, the relative delay induced by the ionization process, plotted in Fig. 10b, is also correct up to a constant.

The relative atomic phase of the ionization process decreases in magnitude as the photon energy increases and has an asymptotic behavior as it reaches far above the ionization threshold (see Fig. 6). The detection gases used in our experiment have different ionization thresholds; we therefore observe a nonvanishing difference between them, especially close above the ionization potential of neon, where the relative atomic phase in the argon is already flattening out. Although the influence of the atomic phases remains small over the range investigated, it is visible experimentally, and the agreement with theoretical data is rather good. With these measurements we have taken a first step in the direction of probing the fundamental process—photoionization—in the time domain with attosecond resolution.

4. ATTOSECOND PULSE TRAINS CREATED BY SUB-10-FEMTOSECOND LASER PULSES

Figure 11 presents RABITT measurements obtained in argon using postcompressed laser pulses (see Section 3.2). The intensity was estimated to be 8×10^{13} W/cm^2, and the duration of the IR pulses was found to be ≈9 fs by SPIDER measurements. As expected, the spectral lines are broadened compared to Fig. 5 and the number of oscillations as a function of delay is reduced, since both pulses are considerably reduced in duration. From the cross-correlation measurements of Fig. 11, we can give an upper limit for the duration of the APT, namely, 3 fs, which is consistent with what can be expected for harmonic generation at the estimated IR intensity.

It is interesting, in this particular case, to reconstruct the complete attosecond pulse train. Unfortunately, RABITT measurements at only one intensity and over a limited total pulse duration do not allow us to provide a complete reconstruction [37] (numerical reconstructions of attosecond pulse trains are discussed in [34, 37, 38]). We present in Fig. 12 a reconstructed pulse train, using an adiabatic approximation for illustration purposes, with the following assumptions: the harmonics are assumed to be Gaussian pulses with a FWHM τ = 3 fs. The APT is reconstructed according to

$$I(t) = \left| \sum_{q = 13, 23} A_q e^{-2\ln 2 t^2/\tau^2} e^{-iq(\omega t + \phi_0) - iq\omega t_q - ib_q t^2} \right|^2. \quad (9)$$

The harmonic amplitudes (A_q) are determined experimentally from the RABITT scan of Fig. 11. The group

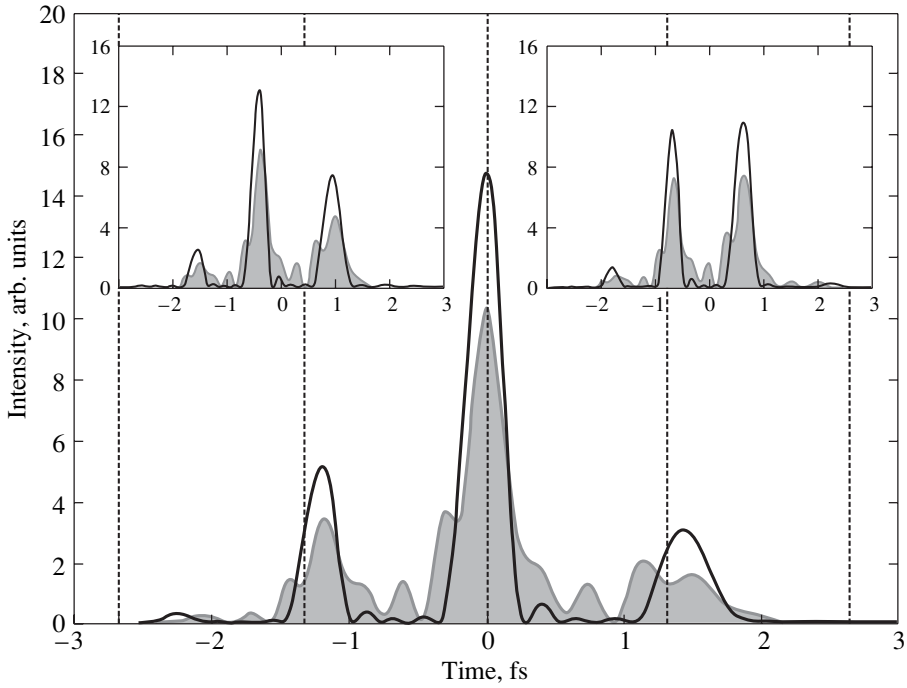

Fig. 12. Representation of an APT produced by a sub-10-fs IR pulse. Dashed lines guide the eye for even spacing. We show, by the gray filled line, the APT we measure on-target after passing through a 200-nm filter. The black line illustrates a train to which we added the effect of an additional 600-nm filter in the calculations. In the experiment, we lack information on the delay between the APT and its envelope. The insets show scenarios with different (arbitrarily set) delays.

delay t_q incorporates the delay due to the generation as well as the delay due to the Al filter. It is determined from Fig. 11 for a 200-nm filter. (We can also simulate the effect of a thicker filter by adding the corresponding group delay.) The experimental data allow us to determine t_q up to a constant, which we include in ϕ_0 together with the unknown absolute phase of the fundamental. This causes a delay uncertainty in the reconstruction, which determines the position of the attosecond pulses under the envelope. We arbitrarily chose the value of ϕ_0 and show three situations in Fig. 12. The harmonic chirp b_q is calculated using the strong-field approximation [35].

For this rather low generating intensity, the large chirp [12] of the attosecond pulses almost completely suppresses the attosecond pulse train structure. We show the train with the measured phase difference (including the passage through a 200-nm Al filter) by the gray filled line in Fig. 12. The production of short attosecond pulses in this case requires the insertion of an additional 600-nm-thick Al filter, as shown by the black curve. As seen in Fig. 12, for the optimal delay, there is either only one main attosecond burst with two satellites or two main bursts for other delays. The time interval between two consecutive attosecond pulses increases during the total XUV pulse [18, 35]. This is a consequence of the negative chirp exhibited by the harmonics. The pulse duration of the attosecond pulses is shortest at the pulse maximum and increases on the wings [39].

5. CONCLUSION

In conclusion, we have presented a series of experimental measurements of attosecond pulse trains. We have shown that it is possible to manipulate the pulse duration of individual attosecond pulses by passing them through appropriate metallic filters. We have discussed the possibility of using the broadband coherent harmonic spectrum for group delay measurements of thin films and for characterizing the ionization process. Finally, we have presented a recent result obtained with very short (9-fs) infrared pulses.

ACKNOWLEDGMENTS

This research was supported by a Marie Curie Intra-European Fellowship (MEIF-CT-2004-009268), the Marie Curie Research Training Network XTRA (MRTN-CT-2003-505138), the Integrated Initiative of Infrastructure LASERLAB-EUROPE (RII3-CT-2003-506350, FOSCIL) within the 6th European Community Framework Program, the Knut and Alice Wallenberg Foundation, the Swedish Science Council, the Swedish Foundation for International Cooperation in Research and Higher Education (STINT-IG2003-2057), and the National Science Foundation. Discussions with M. Iva-

nov, Y. Mairesse, and P. Salieres are gratefully acknowledged. K.V. is on leave from the Department of Optics and Quantum Electronics, University of Szeged, Szeged, Hungary. R.L-M is currently at Laboratoire d'Optique Appliquée, ENSTA, France.

REFERENCES

1. M. Ferray, A. L'Huillier, X. F. Li, *et al.*, J. Phys. B **21**, L31 (1988).
2. Gy. Farkas and Cs. Toth, Phys. Lett. A **168**, 447 (1992).
3. S. E. Harris, J. J. Macklin, and T. W. Hänsch, Opt. Commun. **100**, 487 (1993).
4. P. Tzallas, D. Charalambidis, N. A. Papadogiannis, *et al.*, Nature **426**, 267 (2003).
5. M. Hentschel, R. Kienberger, Ch. Spielmann, *et al.*, Nature **414**, 509 (2001).
6. R. Kienberger, M. Hentschel, M. Uiberacker, *et al.*, Science **297**, 1144 (2002).
7. R. Kienberger, E. Goulielmakis, M. Uiberacker, *et al.*, Nature **427**, 817 (2004).
8. A. Baltuška, Th. Udem, M. Uiberacker, *et al.*, Nature **421**, 611 (2003).
9. P. M. Paul, E. S. Toma, P. Breger, *et al.*, Science **292**, 1689–1692 (2001).
10. H. G. Muller, Appl. Phys. B **74**, S17 (2002).
11. R. López-Martens, K. Varjú, P. Johnsson, *et al.*, Phys. Rev. Lett. **94**, 033001 (2005).
12. Y. Mairesse, A. de Bohan, L. J. Frasinski, *et al.*, Science **302**, 1540 (2003).
13. M. Bellini, C. Lynga, A. Tozzi, *et al.*, Phys. Rev. Lett. **81**, 297 (1998).
14. P. Salières, B. Carré, L. Le Déroff, *et al.*, Science **292**, 902 (2001).
15. P. Tournois, Opt. Commun. **140**, 245 (1997).
16. S. Sartania, Z. Cheng, M. Lenzner, *et al.*, Opt. Lett. **22**, 1562 (1997).
17. M. Nisoli, S. De Silvestri, O. Svelto, *et al.*, Opt. Lett. **22**, 522 (1997).
18. J. Mauritsson, R. López-Martens, P. Johnsson, *et al.*, Phys. Rev. A **70**, 021801(R) (2004).
19. C. Iaconis and I. A. Walmsley, Opt. Lett. **23**, 792 (1998).
20. W. Kornelis, J. Biegert, J. W. G. Tisch, *et al.*, Opt. Lett. **28**, 281 (2003).
21. R. López-Martens, J. Mauritsson, P. Johnsson, *et al.*, Phys. Rev. A **69**, 053811 (2004).
22. P. O'Keeffe, R. López-Martens, J. Mauritsson, *et al.*, Phys. Rev. A **69**, 051401(R) (2004).
23. D. J. Kennedy and S. T. Manson, Phys. Rev. A **8**, 227 (1972).
24. E. S. Toma and H. G. Muller, J. Phys. B **35**, 3435 (2002).
25. J. Mauritsson, M. B. Gaarde, and K. J. Schafer (in preparation).
26. K. T. Kim, C. M. Kim, M.-G. Baik, *et al.*, Phys. Rev. A **60**, 051805(R) (2004).
27. Y. Mairesse, A. de Bohan, L. J. Frasinski, *et al.*, Phys. Rev. Lett. **93**, 163901 (2004).
28. Of course, knowing the optimal thickness for the filter the intensity of the pulses can be significantly enhanced by only using one filter of the correct thickness, thereby reducing the number of surfaces covered by Al_2O_3 from six to two.
29. D. Y. Smith, E. Shiles, and M. Inokuti, in *Handbook of Optical Constants of Solids*, Ed. by E. D. Palik (Academic, Orlando, 1985), pp. 369–398.
30. F. Gervais, in *Handbook of Optical Constants of Solids II,* Ed. by E. D. Palik (Academic, San Diego, 1991), pp. 761–775.
31. D. Descamps, L. Lyngå, J. Norin, *et al.*, Opt. Lett. **25**, 135–137 (2000).
32. http: //www.cxro.lbl.gov/optical-constants/.
33. V. Véniard, R. Taïeb, and A. Maquet, Phys. Rev. A **54**, 721 (1996).
34. F. Quéré, Y. Mairesse, and I. Itatani, J. Mod. Opt. **52**, 339 (2005).
35. K. Varjú, Y. Mairesse, B. Carré, *et al.*, J. Mod. Opt. **52**, 379 (2005).
36. L. C. Dinu, H. G. Muller, S. Kazamias, *et al.*, Phys. Rev. Lett. **91**, 063901 (2003).
37. Y. Mairesse *et al.* (in preparation).
38. J. Mauritsson *et al.* (in preparation).
39. K. Varjú *et al.* (in preparation).